Intestinal RICT-1/Rictor regulates larval germline progenitors via vitellogenins VIT-1 and VIT-3 in *C. elegans*

Running title: *rict-1* regulates germline development via vitellogenins

Anke Kloock,
E. Jane Albert Hubbard*

Department of Cell Biology,
NYU Grossman School of Medicine
New York, NY 10016

*Corresponding author

Keywords: TORC2, Stem Cells, Rictor, Vitellogenin, germ line

ABSTRACT

Highly conserved signaling pathways communicate cellular and organismal nutrient conditions to proliferating pools of cells such as stem cells and tumors. One such pathway is the Target of Rapamycin (TOR) pathway. The TOR kinase exists in two complexes, TOR complex 1 (TORC1) and TOR complex 2 (TORC2). In the *Caenorhabditis elegans* hermaphrodite, TORC1 signaling cell-autonomously promotes the establishment of the larval germline Progenitor Zone (PZ). Here, we show that RICT-1, the sole *C. elegans* ortholog of the TORC2-specific component Rictor, also promotes expansion of the larval PZ through canonical TORC2 signaling. Unlike the TORC1 components, intestinal *rict-1* is both necessary and sufficient for full germline PZ pool establishment. Comparative RNA-seq on staged L4 larvae indicates that intestinal RICT-1 likely acts via vitellogenins. These intestinally produced yolk proteins provision oocytes, but they were not previously known to act in larval germ line development. Genetic analysis supports roles for *vit-1* and *vit-3* in a linear pathway with *rict-1*. Our results establish the *C. elegans* germ line as a fruitful model for investigating TORC2 and its connection to stem cells and lipid biology.

<u>Summary Statement</u>

RICT-1/Rictor in *C. elegans* promotes larval germline development via canonical TORC2 signaling, and intestinal RICT-1 acts via vitellogenins VIT-1 and VIT-3 to promote the establishment of the germline progenitor pool.

INTRODUCTION

Highly conserved signaling pathways govern cellular responses to nutrients and metabolites. These responses are required for the proper regulation of pools of proliferating cells such as stem cells and tumor cells (Puca et al., 2022; Tu et al., 2023).

TOR is a highly conserved serine/threonine kinase that is conserved from yeast to mammals and integrates nutritional signals to regulate cellular responses (reviewed in (Liu and Sabatini, 2020)). TOR acts in two complexes bearing key subunits Raptor in TORC1 and Rictor in TORC2. Both complexes respond to nutritional signals and regulate many nutrient-dependent aspects of stem cell biology (reviewed in (Russell et al., 2011; Saba et al., 2021)). Albeit differently, both complexes respond to amino acid availability and impact lipid metabolism (reviewed in (Caron et al., 2015; Szwed et al., 2021; Zoncu et al., 2011)) and homeostasis (Kim and Chen, 2004). TORC2 furthermore promotes *de novo* fatty acid and lipid synthesis in mice (Guri et al., 2017) and worms (Jones et al., 2009; Soukas et al., 2009). In *C. elegans,* our prior work established that TORC1 components and/or downstream effectors affect germline stem cell proliferation and differentiation germ line-autonomously and in response to amino acid provision (Korta et al., 2012; Roy et al., 2018).

Reducing Rictor activity in rodents, worms, or flies results in small animals that develop slower (Guertin et al., 2006; Hietakangas and Cohen, 2007; Jones et al., 2009; Soukas et al., 2009). Rictor mutants in rodents and worms accumulate fat (Frei et al., 2023; Jones et al., 2009; Soukas et al., 2009; Yen et al., 2010), suggesting Rictor may facilitate trafficking of lipids from the intestine to other organs (Jones et al., 2009; Soukas et al., 2009). Adult *C. elegans* hermaphrodites bearing mutations in *rict-1*, the sole Rictor ortholog (Jones et al., 2009), exhibit reduced intestinal expression of the vitellogenin gene *vit-3* (Breen et al., 2024; Dowen et al., 2016) and produce fewer offspring (Jones et al., 2009; Soukas et al., 2009; Webster et al., 2013).

A pool of stem and progenitor cells, known collectively as the progenitor zone (PZ) pool, exists in the distal part of the hermaphrodite gonad (reviewed in (Hubbard and Schedl, 2019)), and the PZ pool is related to offspring production in sperm-replete worms (Agarwal et al., 2018; Kocsisova et al., 2019). The PZ is maintained by Notch pathway signaling via direct activation of downstream targets *sygl-1* and *lst-1* (Chen et al., 2020;

Kershner et al., 2014) that interfere with three partially redundant differentiation pathways (Mohammad et al., 2018).

Our results show that *rict-1* mutant worms accumulate half the normal number of cells in the PZ during larval stages and have a reduced number of offspring. As in other phenotypic contexts, *rict-1* acts via *sinh-1* and *sgk-1*. However, in this role, *rict-1* does not act via the IIS or TGF-ß pathways which are implicated in larval PZ expansion (Dalfó et al., 2012; Michaelson et al., 2010; Pekar et al., 2017) and in *rict-1* control of dauer entry (O'Donnell et al., 2018). Loss of *rict-1* reduces the average mitotic index in larvae and likely acts in parallel to GLP-1. We show that intestinal RICT-1 is sufficient and necessary for full establishment of the adult PZ. Our transcriptomics analysis indicates that during the L4 larval stage, *rict-1* regulates expression of several members of the conserved ApolipoproteinB-like vitellogenin family (reviewed in (Perez and Lehner, 2019)), and that *vit-1* and *vit-3* contribute to expansion of the progenitor pool, likely downstream of *rict-1*.

RESULTS

RICT-1 is required for normal germline development

To explore effects of TORC2 on the germ line, we examined the effects of reduced *rict-1.* We first assessed phenotypes in two *rict-1* mutants (*ft7* in the third exon and *mg360* in the 11th exon (Jones et al., 2009; Soukas et al., 2009)), in 6 additional alleles that we generated using CRISPR-Cas9 genome editing, and in an additional deletion mutant (Breen et al., 2024). Among three different isoforms *ft7* only affects isoforms A and B, while *mg360* affects all three (Fig. 1A). We generated four CRISPR mutants with Stop-In cassettes (Wang et al., 2018) inserted in the regions of each of the SNPs: *na112* and *na113* in the third exon, and *na11*4 and *na115* in the 11th exon. We also generated two additional mutants: one that deletes 241bp of the 5'UTR and 29bp of the first exon (*na116*), and one that deletes 520bp in total across the first three exons (*na119*). We used the Stop-In strategy so as not to interfere with the *pqn-32* locus that resides within the intron between exons 10 and 11. We furthermore assessed a mutant that deletes both *rict-1* and *pqn-32* (Breen et al., 2024).

To gauge the effects of *rict-1* on larval accumulation of the stem/progenitor pool, we counted the number of nuclei per distal gonad arm in the distal progenitor zone (PZ) at the L4-to-adult molt. We chose to assess the progenitor pool at the molt because this represents a developmental timepoint that is independent of growth rate and is at the start of the early adult steady-state PZ pool (reviewed in (Hubbard and Schedl, 2019)). All nine *rict-1* mutants displayed a similar significant reduction in the number of PZ nuclei, reaching half of the wild-type level (average 106.2 $\pm$ 1.00 across all nine alleles versus 196.6 $\pm$ 3.08 in the wild type) (Fig. 1B-D). Given that all *rict-1* mutants behaved similarly, our subsequent studies used the *na113* allele, indicated as *rict-1(-)* hereafter.

The brood size in mated worms is correlates with the number of PZ nuclei (Agarwal et al., 2018; Kocsisova et al., 2019). To determine whether the PZ pool reduction we observed in the *rict-1* mutants is associated with reproductive defects, we assessed live broods and, consistent with previous results (Jones et al., 2009; Soukas et al., 2009), we observed a significantly smaller number of hatched offspring for both *rict-1* alleles tested (199.2 $\pm$ 9.21 for *rict-1(ft7)* and 199.8 $\pm$ 3.81 for *rict-1(na113)*) compared with the wild type

120 (312.8 ± 6.77) (Fig. 1E,F). We also observed that *rict-1* mutants display an extended
121 reproductive span of ~9 days compared with ~6 days in the wild type (9.0 ± 0.41 days for
122 *rict-1(na113)*, 9.2 ± 0.49 for *rict-1(ft7)*, and 6.4 ± 0.31 for the wild type (Fig. 1F,G)),
123 consistent with previous results (Webster et al., 2013). Since hermaphrodite brood size
124 is sperm limited (Hodgkin and Barnes, 1991), and the correlation with the PZ can only be
125 assessed in the presence of replete sperm, we assessed live broods in mated worms.
126 We found that, unlike the wild type, where male sperm provision significantly increased
127 offspring number, the number of hatched offspring is not increased in mated *rict-1*
128 mutants (Fig. S1). Despite the extended reproductive period, the overall sum of hatched
129 brood of *rict-1* mutants is still reduced relative to wild type (Fig. 1F). We conclude that
130 RICT-1 promotes normal germline development, and we focused on the PZ pool
131 phenotype as this is a primary early aspect of germline development.
132
133 **RICT-1 acts through canonical TORC2 to establish the early adult PZ pool**
134 We next assessed known pathway components or downstream effectors of the
135 canonical TORC2 complex. Canonically, Rictor and SINH-1 are in the TORC2 complex,
136 and TORC2 activates SGK (reviewed in (Blackwell et al., 2019; Jang et al., 2022)).
137 In *C. elegans*, SINH-1 acts similarly to Rictor in many phenotypic contexts
138 (Aspernig et al., 2019; Emans et al., 2023; McLachlan et al., 2022). To test if RICT-1 is
139 acting through canonical TORC2 to establish the larval PZ, we assessed the number of
140 PZ nuclei in worms bearing mutations in *rict-1(-)* or *sinh-1(-)* or both (Fig. 2A). We found
141 that the number of PZ nuclei was similarly reduced in each single mutant and in the double
142 mutant (104.7 ± 3.35, 114.3 ± 3.68, and 107.8 ± 3.25, respectively). These results are
143 consistent with RICT-1 and SINH-1 acting in the same complex.
144 In *C. elegans*, SGK-1 acts genetically downstream of Rictor in many phenotypic
145 contexts (Aspernig et al., 2019; Dowen et al., 2016; Emans et al., 2023; Gatsi et al., 2014;
146 Jones et al., 2009; Ruf et al., 2013; Soukas et al., 2009; Webster et al., 2013). To
147 determine whether a similar genetic interaction exists for PZ establishment, we compared
148 PZ counts in the null single and double mutants. We found that the number of PZ nuclei
149 is similar in *rict-1* or *sgk-1* single mutants (108.8 ± 3.17 and 104.5 ± 2.15 for *rict-1(-)* and
150 *sgk-1(-)*, respectively) and in the *rict-1; sgk-1* double mutant (94.7 ± 2.15) (Fig. 2B). While

151 PZ counts in each single mutant do not differ, the *rict-1*; *sgk-1* double mutant is modestly,
152 but significantly, lower than in the *rict-1* mutant alone (p=0.024). This result suggests that
153 while *sgk-1* is likely acting downstream of *rict-1*, it may have additional *rict-1*-independent
154 minor effects on the PZ phenotype independent of *rict-1* (Fig. 2B).
155 An *sgk-1* gain-of-function allele (*gf*) (Jones et al., 2009) fully (Jones et al., 2009;
156 Sakai et al., 2017) or partially (Aspernig et al., 2019; Ruf et al., 2013) suppresses *rict-1*
157 mutant phenotypes, consistent with a role for SGK-1 downstream of RICT-1 (Jones et al.,
158 2009; Sakai et al., 2017). To determine whether the *sgk-1(gf)* mutant suppresses the
159 *rict-1* mutant PZ phenotype, we examined *sgk-1(gf)* alone and in combination with
160 *rict-1(-).* We found that *sgk-1(gf)* alone displays a PZ count similar to the wild type (178.7
161 ± 5.10 versus 189.8 ± 4.06). As expected if SGK-1 were acting downstream of RICT-1,
162 we found significant, though partial, suppression of the *rict-1* PZ phenotype (to 124.1 ±
163 3.48 PZ nuclei). Taking the loss- and gain-of-function results together, we conclude that
164 SGK-1 likely acts downstream of RICT-1, even though the two may have other minor
165 independent outputs that affect the PZ phenotype.
166
167 **RICT-1 does not act via DAF-2/IIS or DAF-7/TGF-ß pathways to promote**
168 **accumulation of the larval progenitor pool**
169 In the phenotypic context of dauer entry, intestinal *rict-1* signals via neuronal
170 DAF-28 Insulin and DAF-7 TGF-ß from ASI and ASJ (O'Donnell et al., 2018). This finding
171 was of particular interest to us since we previously characterized roles for both the IIS
172 and TGF-ß pathways in establishing the PZ pool (Dalfó et al., 2012; Michaelson et al.,
173 2010; Pekar et al., 2017). In both pathways, these same neurons are implicated: *ins-3* is
174 implicated upstream of DAF-2 for PZ phenotypes and is expressed in ASI and ASJ
175 (Ghaddar et al., 2023; Michaelson et al., 2010), while ASI is implicated by cell ablation for
176 the DAF-7 pathway regulation of the germ line stem cell niche (Dalfó et al., 2012).
177 Importantly, the PZ accumulation defect upon reduced *daf-2* or *daf-7* is fully suppressible
178 by loss of *daf-16* or *daf-3*, respectively.
179 If the relevant IIS and/or TGF-ß pathways mediate the effects of *rict-1* on the PZ,
180 we would expect loss of *daf-16* and/or *daf-3* to suppress the *rict-1* mutant PZ defect. To
181 test this hypothesis, we constructed strains bearing double or triple mutants of *rict-1(-)*

182 with *daf-16(-)* and/or *daf-3(-)* and counted the number of nuclei in the PZ pool. We found
183 that neither *daf-16(-)* nor *daf-3(-)* alone strongly suppressed the PZ defect in the *rict-1*
184 mutant (Fig. 3A). The PZ of the *daf-16(-); rict-1(-)* averaged 119.1 ± 2.91 (compared with
185 97.6 ± 2.73 for *rict-1(-)* alone). While this small difference is statistically significant, we
186 note that *daf-16(-)* has a greater (though not statistically significant) average number of
187 PZ nuclei than the wild type (Fig. 3A). For the DAF-7/TGFß pathway, we found that the
188 PZ pool of *daf-3(-); rict-1(-)* was not significantly different from the *rict-1* mutant alone.
189 Most important, the triple mutant *daf-16(-); rict-1(-); daf-3(-)* averages the same number
190 of PZ nuclei (109.0 ± 2.54) as either double mutant or the *rict-1(-)* mutant alone (Fig. 3A).
191 We conclude from these results that neither DAF-2/IIS (via DAF-16) nor DAF-7/TGFß
192 pathways mediate the effects of RICT-1 on PZ accumulation.
193
194 **RICT-1 promotes larval cell cycle progression, but does not enhance the Glp-1-like**
195 **"loss of progenitor pool" phenotype**
196 Our prior work established that *rsks-1/*S6K affects both the cell cycle and cell fate
197 in the PZ (Korta et al., 2012; Roy et al., 2016). Loss of *rsks-1* reduces both larval mitotic
198 index and S phase index, as well as on the proportion of cells in G1 or G2, suggesting a
199 generally slower cell cycle in the mutant. These reductions were observed in the mid-L4
200 stage larvae when the PZ is still expanding, however no differences were observed in the
201 adult homeostatic stage when the cell cycle is already slowed relative to larval stages.
202 Moreover, in combination with a reduction of *glp-1* (using a temperature-sensitive allele
203 at a semi-permissive temperature), loss of *rsks-1* had a dramatic effect on the PZ such
204 that in over 50% of *glp-1(ts) rsks-1(sv31)* double mutants at 20ºC, all germ cells had
205 differentiated, mimicking a complete loss of *glp-1* and demonstrating a parallel role for
206 *rsks-1* in cell fate (Korta et al., 2012; Roy et al., 2016).
207 To determine how *rict-1* affects cell cycle and cell fate, we assessed the mitotic
208 index in the *rict-1(-)* mutant in mid-L4 stage larvae and found that, similar to *rsks-1,* the
209 larval mitotic index was reduced in *rict-1(-)* mutants (2.23 ± 0.16 for *rict-1(-)* mutants
210 versus 2.85 ± 0.23 for wild-type (Fig. 3B)). Similar to prior results with *rsks-1, rict-1* does
211 not affect the mitotic index in adults (Fig. S2A).

212 Furthermore, we assessed the genetic interaction with *glp-1*. Unlike what was
213 observed with *rsks-1*, the double *glp-1(ts); rict-1(-)* mutant did not cause differentiation of
214 the entire PZ (Fig. 3C). However, the double mutant (*rict-1(-); glp-1(ts)*) showed a minor
215 increase in the percentage of gonad arms with fewer than 50 PZ nuclei (39% of gonad
216 arms for the *rict-1(-); glp-1(ts)* mutant with <50 PZ nuclei, versus 0% for each single
217 mutant) (Fig. 3B). This suggests that RICT-1 acts in parallel to *glp-1* (Fig. 3B).
218 Furthermore, the number of PZ nuclei for the double mutant of *rict-1(-)* and *glp-1(ts)* is
219 additive (Fig. S2B). Together, these results support the conclusion that RICT-1 is acting
220 to promote robust larval cell cycle progression but does not affect the stem cell fate
221 decision.
222 Within the PZ pool there are distal SYGL-1(+) stem cells (Shin et al., 2017) and
223 more proximal SYGL-1(-) progenitors that are completing a final round of mitosis (Fox
224 and Schedl, 2015). We asked whether loss of *rict-1* affects these early adult pools
225 independently. Using as a readout the distance from the distal end of the gonad to the
226 proximal border of each pool, we found that *rict-1(-)* mutants had a significantly shorter
227 SYGL-1(+) zone than wild-type worms ($p<0.001$, 48.3 ± 0.96 μm versus 56.0 ± 0.96 μm,
228 respectively) (Fig. 3C). The length of the PZ was also reduced in *rict-1(-)* mutants in
229 comparison to wild-type worms ($p<0.001$, 87.0 ± 1.24 versus 105.2 ± 1.44, respectively)
230 (Fig. 3D). When we assessed the relative length of the SYGL-1(+) zone to the PZ, we
231 observed that in both strains the SYGL-1(+) zone is about half the length of the PZ (0.55
232 $\pm$ 0.013 for *rict-1(-)* mutants and 0.53 ± 0.009 for the wild type) (Fig. 3E). These results
233 suggest that the loss of robust cell cycle progression in larval stages affects both the stem
234 and non-stem-progenitor portions of the adult PZ pool.
235
236 **Intestinal RICT-1 contributes to PZ pool establishment**
237 In several different phenotypic contexts, *rict-1* acts from the intestine. These
238 contexts include dauer entry and foraging behavior (O'Donnell et al., 2018), associative
239 learning (Sakai et al., 2017), fat accumulation (Jones et al., 2009; Soukas et al., 2009),
240 and food seeking (McLachlan et al., 2022). Single cell RNA-seq analyses show that *rict-*
241 *1* mRNA is widely expressed but is most highly abundant in the intestine (Fig. S3A from
242 (Cao et al., 2017; Hutter and Suh, 2016)).

243 We therefore asked whether intestinal RICT-1 might influence PZ pool
244 establishment. To test this, we depleted RICT-1 in the intestine using tissue-specific
245 auxin-mediated protein degradation(Zhang et al., 2015). We generated a sAID::RICT-1
246 fusion (*rict-1(na117)*) by CRISPR-Cas9 genome editing, and determined that it does not
247 impact protein function, as the number of PZ nuclei is not significantly different from that
248 of wild-type worms (Fig. S3B). We then crossed this allele into a strain in which TIR1 is
249 driven by the intestine-specific promoter *ges-1p.* We observed that in the presence of
250 auxin, the number of PZ nuclei is significantly reduced (153.3 ± 3.23 with auxin vs. 189.7
251 ± 3.21 without auxin). Neither the vehicle (EtOH) nor auxin alone affected the PZ counts
252 of the other strains tested (wild type, *rict-1(-)*, *rict-1(na117*[sAID::RICT-1]) or *ieSi61*[*ges-*
253 *1p*::TIR1] alone), indicating that the lower PZ count we observed in the presence of the
254 TIR1 and auxin is due to auxin-induced protein degradation and not to auxin-induced
255 stress (Fig. 4A).
256 To determine whether intestinal *rict-1(+)* is sufficient to promote accumulation of
257 the larval PZ pool, we expressed *rict-1(+)* from an intestinal promoter, *ges-1p,* on an
258 extrachromosomal array in the *rict-1(-)* background. We found that the array-bearing
259 siblings contain a significantly greater number of PZ nuclei (145.2 ± 3.73) than their non-
260 array-bearing siblings (100.6 ± 3.48). In addition, there is no difference between the PZ
261 counts of non-array bearing progeny of array-bearing mothers and homozygous
262 *rict-1(-)* mutants (Tukey comparison p=0.533). This result supports the conclusion that
263 maternal effects do not contribute to *rict-1* regulation of the PZ (Fig. 4B).
264 Taken together, our necessity and sufficiency tests demonstrate that intestinal
265 RICT-1 is a major contributor to the accumulation of the larval PZ pool. Interestingly,
266 intestinal degradation of RICT-1 does not lower the number of PZ nuclei to the level of
267 the *rict-1(-)* (Fig. 4A), nor does intestinally-expressed *rict-1* entirely rescue to wild-type
268 levels (Fig. 4B). These results indicate that either degradation and heterologous rescue
269 do not reach null or wild-type levels, respectively, or that RICT-1 acts in additional tissues.
270 Single cell RNA-seq analysis (Fig. S3A, data from (Cao et al., 2017; Hutter and
271 Suh, 2016)) indicates that in addition to the intestine, larval *rict-1* is expressed in other
272 tissues, including the germ line. Given our prior results indicating a role for TOR in the
273 germ line (Korta et al., 2012) we tested RICT-1 germline degradation using *ieSi38*[*sun-*

274 *1p*::TIR1] and found that it also contributes, though less than the intestine (Fig. S3C). We
275 conclude that although other tissues contribute, the intestine is the primary source of
276 RICT-1 that is important for establishment of the early adult germline PZ, with additional
277 contribution from the germ line.
278
279 **Transcripts of four vitellogenin-encoding genes are depleted in the *rict-1(-)* mutant**
280 **relative to wild type at the mid-L4**
281 To determine how *rict-1* influences the larval germ line, we performed comparative
282 bulk RNA-sequencing in biological triplicate of three strains of tightly synchronized mid-
283 L4 stage worms: wild type, the *rict-1(-)* mutant, and the *rict-1(-)* mutant in which *rict-1(+)*
284 is expressed solely in the intestine. We integrated the extrachromosomal array and
285 determined that the resulting strain was functional and displayed a similar PZ phenotype
286 to worms with *Ex[intestinal rict-1(+)]* (Fig.S3C). This combination of strains allowed us to
287 explore the impact of both global and intestine-specific activity of *rict-1* on the
288 transcriptome. The PCA analysis for all three strains indicates that all three strains are
289 distinctly different from each other (Fig. 5A).
290 Comparing the *rict-1* mutant and the wild type, we found that among 16,034 protein
291 coding transcripts detected (see Methods), 151 transcripts were differentially abundant
292 (adjusted $p < 0.05$ and log2 fold change >2), with 44 less abundant and 107 more
293 abundant in the *rict-1(-)* mutant than in the wild type (Fig. 5B). Among the genes with
294 lower transcript abundance in the mutant, the vitellogenin genes caught our attention for
295 several reasons. The *C. elegans* genome encodes six vitellogenins, members of a family
296 of conserved yolk proteins (reviewed in (Perez and Lehner, 2019)) that are best described
297 for their adult function provisioning oocytes (Grant and Hirsh, 1999; Kimble and Sharrock,
298 1983). However, no function in larval stages or the larval germ line is yet described. We
299 found that the steady-state mRNA levels of four of the six vitellogenins (*vit-1, -3, -4,* and
300 *-5*) are significantly lower in the mid-L4 *rict-1* mutant relative to wild type (adjusted
301 $p<0.001$, log2 fold change < -2) (Fig. 5B, orange circles).
302 To assess the contribution of intestinal *rict-1(+)*, we then analyzed the 151
303 transcripts to determine which of these were significantly different between the mutant
304 alone and the strain expressing *rict-1(+)* solely in the intestine (Fig. 5C). We found that a

305 third of these 151 transcripts were significantly different between the global *rict-1* mutant
306 versus *rict-1* mutants expressing *rict-1(+)* only in the intestine: 18 were higher and 35
307 were lower for *rict-1(-)* versus *rict-1(-); Is[intestinal rict-1(+)]* (Fig. 5D, upper left and lower
308 right, respectively). Interestingly, transcripts of two of the *vit* genes (*vit-1* and *vit-3)* are
309 significantly higher in the *rict-1(-)* mutant expressing intestinal *rict-1(+)* relative to the
310 *rict-1(-)* mutant alone (Fig. 5D), suggesting that their expression may be regulated by
311 intestinal *rict-1*.
312
313 **VIT-1 and VIT-3 promote germline progenitor pool establishment**
314 We wished to determine the functional relevance of VIT-1 and VIT-3 to progenitor
315 zone establishment in larvae. Among the vitellogenin genes we detected in our
316 comparative RNA-seq analysis, *rict-1* was previously found to indirectly regulate *vit-3*
317 transcription in the adult intestine (Breen et al., 2024; Dowen et al., 2016). However, no
318 previous function has been described in larvae for any of the vitellogenins, and no
319 previous connection has been made between *vit-1* and *rict-1*.
320 We therefore tested whether VIT-1 and VIT-3 could, like RICT-1, contribute to PZ
321 pool establishment, by counting the number of PZ nuclei in worms bearing loss-of-
322 function alleles of *vit-1* or *vit-3*. We observed that *vit-1(-)* and *vit-3(-)* null mutants each
323 contain significantly fewer PZ nuclei (138.1 ± 4.84 and 130.45 ± 2.30, respectively) than
324 the wild type (179.6 ± 5.62 and 202.9 ± 5.35) (Fig. 6A,B).
325 If *rict-1* and either *vit* gene were acting in a linear genetic pathway, we would expect
326 that loss of both *rict-1* and either *vit* gene would not further deplete the PZ pool beyond
327 either the *rict-1* or *vit* single mutant alone. We found that the double mutant *rict-1(-); vit-*
328 *1(-)* and the double mutant *rict-1(-); vit-3(-)* each display the same number of PZ nuclei
329 as the *rict-1(-)* mutant alone (96.0 ± 2.38 for *rict-1(-); vit-1(-) versus* 102.3± 2.96 for *rict-*
330 *1(-)* alone, and 108.7 ± 3.40 for *rict-1(-); vit-3(-)* versus 99.5± 3.10 for *rict-1(-)*). Together,
331 these results are consistent with a linear genetic pathway and reveal an unexpected role
332 for *vit-1* and vit-*3* in the larval accumulation of germline progenitors, likely downstream of
333 *rict-1.*

334 **DISCUSSION**

335 This work establishes a developmental context for a novel non-autonomous
336 activity of intestinal RICT1/Rictor on a stem cell system. In addition, it indicates a role for
337 vitellogenins downstream of intestinal RICT-1 in establishment of the germline progenitor
338 pool. In the course of this work, we generated seven new alleles of *rict-1*, including six
339 similarly-behaving alleles encoding small deletions or early stop codons, and one
340 encoding a functional AID-tagged RICT-1 protein. Using these and prior existing alleles,
341 we show that RICT-1 is required for several aspects of germline development and
342 reproduction.

343 Using multiple mutant alleles of *rict-1*, we confirmed low broods reported by others
344 (Jones et al., 2009; Soukas et al., 2009), and we also confirmed an extended period of
345 progeny production (Webster et al., 2013). Interestingly, we observed no increase of
346 progeny production upon replete sperm provision, suggesting that sperm is not the
347 limiting factor for offspring production in the *rict-1* mutant. In mated worms, brood size
348 correlates with an increased number of cells in the PZ pool, suggesting that the number
349 of PZ cells destined to become oocytes is limiting (Agarwal et al., 2018; Kocsisova et al.,
350 2019). We speculate that a similar limitation could account for our observation.

351 We focused on a larval requirement for RICT-1 in the accumulation of germline
352 progenitors and determined that the *rict-1* mutant PZ pool reaches half the normal number
353 of cells at the adult molt. Multiple *rict-1* mutants affecting different areas of the protein
354 displayed similarly reduced PZ numbers (~half of the wild-type). The N-terminus and third
355 exon mutants disrupt only isoform A and B but nevertheless display the same PZ
356 phenotype as those mutants that affect all three isoforms. This suggests that the
357 C isoform is unlikely to play a specific role in the establishment of the PZ.

358 We observed a similarly-reduced PZ phenotype upon loss of SINH-1, a part of the
359 canonical TORC2 complex, and SGK-1, a canonical TORC2 effector, and found evidence
360 for genetically linear relationships with *rict-1.* By contrast, we find no obvious genetic
361 interaction with the DAF-2/IIS or DAF-7/TGF-ß pathways. We find that RICT-1 promotes
362 robust larval, but not adult, germline cell cycle progression but does not affect the stem
363 cell fate decision.

364 While both TORC1 and TORC2 are implicated in progenitor pool establishment,
365 our work reveals interesting differences. We previously found that loss of RSKS-1/S6K,
366 a presumed downstream effector of TORC1, has a similarly reduced PZ as RICT-1, and
367 that the requirement for *rsks-1(+)* is germline-autonomous (Korta et al., 2012). By
368 contrast, although we observed a minor germline-autonomous effect, *rict-1* has a strong
369 non-autonomous (intestine-specific) effect on the germ line. In addition, loss of either *rict-*
370 *1* or *rsks-1* results in reduced larval, but not adult, mitotic index. The reduced larval mitotic
371 index was observed at a time when the cell cycle is relatively short and the mitotic index
372 higher, while the unchanged adult mitotic index was observed at a time when the cell
373 cycle is longer and the mitotic index lower (Roy et al., 2016). However, in contrast with
374 *rsks-1*, loss of *rict-1* does not affect the stem cell fate decision. That is, while loss of *rict-*
375 *1* additively reduces the number of PZ nuclei in combination with *glp-1(ts)* at a semi
376 permissive temperature, unlike *rsks-1,* it does not enhance the "Glp-1-like" phenotype
377 such that the entire PZ is lost to differentiation. We conclude that RICT-1 promotes robust
378 larval cell cycle progression but not the stem cell fate decision. We nevertheless found
379 that this larval cell cycle role impacts the borders of the early adult stem and non-stem
380 progenitor pools.
381 We discovered a prominent non-autonomous role for intestinal *rict-1* in larval
382 establishment of the germline PZ that is both necessary and sufficient for establishment
383 of the full wild-type PZ pool. The necessity experiments were conducted using an auxin-
384 mediated protein degradation system. Because auxin exposure prolongs lifespan (Loose
385 and Ghazi, 2021) and promotes resistance to endoplasmic reticulum stress (Bhoi et al.,
386 2021), we used a minimal concentration of auxin (1mM) that did not enhance the PZ
387 defect in the *rict-1* mutant nor in other control strains. RICT-1 intestinal sufficiency has
388 been demonstrated for other phenotypes including entry to the dauer stage, foraging
389 behavior (O'Donnell et al., 2018), associative learning (Sakai et al., 2017), fat
390 accumulation (Jones et al., 2009; Soukas et al., 2009), and food seeking (McLachlan et
391 al., 2022). Our results indicate that the intestinal rescue of *rict-1(+)* in the *rict-1(-)*
392 background does not rescue the number of PZ nuclei to the full wild-type level, and that
393 the intestinal degradation does also not reduce the number PZ nuclei from the wild-type
394 level to the *rict-1(-)* level, a difference that is likely attributable to the additional germline-

395 autonomous role for *rict-1* (Fig. S2C). Whether the intestine and germ line are the only
396 required tissues and how the germline-autonomous role interacts with TORC1 function
397 are areas for further investigation.

398 Our comparative RNA-sequencing analysis of L4 larvae identified four vitellogenin
399 genes among transcripts that are less abundant in *rict-1* relative to wild type, among which
400 *vit-1* and *vit-3* are partially restored by expression of intestinal *rict-1(+)* in the *rict-1(-)*
401 mutant background. Published RNA-seq analyses of *rict-1* day 1 adults (Breen et al.,
402 2024; VanDerMolen et al., 2025) found significant differential expression of *vit-1*, *vit-2*,
403 *vit-3*, and *vit-4*. RICT-1 indirectly promotes high levels of *vit-3* transcription in the adult
404 intestine (Breen et al., 2024; Dowen et al., 2016).

405 Although no function has been previously ascribed to vitellogenins in larval stages
406 nor in the germ line prior to adult oocyte provisioning, many studies have examined *vit*
407 regulation, including extensive promoter dissection of *vit-2* (reviewed in (Perez and
408 Lehner, 2019)). In addition, in the L4, *vit-3* expression is regulated by *ins-37*, while *wrt-6*
409 modestly regulates both *vit-1* and *vit-3* (Abete-Luzi et al., 2020). In general, expression of
410 all vitellogenins is low to negligible during early larval stages and increases rapidly during
411 the fourth larval stage and into adulthood, but individual *vit* gene expression dynamics
412 varies somewhat between each gene and across life stages (Boeck et al., 2016; Cao et
413 al., 2017; Heine and Blumenthal, 1986; Hillier et al., 2009; Hutter and Suh, 2016). Taken
414 together, these studies suggest the possibility that despite high sequence similarity
415 between the six vitellogenin-encoding genes (Fig. S4), the *vit* genes may have additional
416 and differential functional roles during larval development.

417 We demonstrate a functional role for *vit-1* and *vit-3* in promoting progenitor pool
418 establishment, likely downstream of *rict-1.* The *vit-1* and *vit-3* mutant PZ defects are
419 similar to, though not as severe as, loss of *rict-1,* and loss of either *vit* mutant does not
420 further enhance loss of *rict-1*. Although loss of either *vit-1* or *vit-3* causes a mutant
421 phenotype somewhat less severe than *rict-1*, other *vits* identified in our RNA-seq analysis,
422 or other *rict-1*-regulated gene products may contribute to PZ expansion. In support of the
423 former hypothesis, we note that the rapid increase in all *vit* gene expression during the
424 L4 stage correlates with the time of rapid expansion of the PZ pool (Killian and Hubbard,
425 2004).

426 We speculate that RICT-1 regulates the establishment of the PZ via intestine-
427 germline transport of lipids or other molecules associated with vitellogenin-containing lipid
428 particles in larval stages. While molecules associated with oocyte-bound vitellogenins
429 likely act as a nutrient source for post-embryonic survival (reviewed in (Perez and Lehner,
430 2019)), our results suggest that vitellogenins may promote germ cell cycle in earlier
431 stages. One possibility is that vitellogenins facilitate transport of critical nutrient lipids,
432 such as cholesterol. Another possibility is that they provide limiting membrane lipids
433 required for the demands of germ cell division. Yet another possibility is that they
434 associate with as-yet unknown moieties such as hormones or with microRNAs which are
435 part of yolk (Aupérin et al., 2025) to direct germline development. The oocyte receptor for
436 vitellogenins, RME-2, is not detectable by immunohistochemistry in the distal gonad
437 during larval stages (Grant and Hirsh, 1999; Salinas et al., 2007), though it is detected in
438 larval stages by both bulk (Boeck et al., 2016; Hillier et al., 2009; Hutter and Suh, 2016)
439 and single-cell RNA-seq (Cao et al., 2017; Hutter and Suh, 2016) studies. However, a
440 function for RME-2 prior to oogenesis has not been tested. Alternatively, a different
441 receptor may fulfill this role in larvae. Additional studies are required to determine how
442 larval vitellogenins participate in the establishment of the PZ pool.
443 In conclusion, we present the first evidence that TORC2 contributes to
444 establishment of the full germline stem/progenitor pool. Our results suggest a model
445 whereby intestinal RICT-1 promotes the expression of vitellogenins that support germline
446 progenitor pool expansion during larval stages. Due to the high conservation of TORC2
447 components, vitellogenins, and their receptors, our results may have general implications
448 for how Rictor and TORC2 regulate germline development in other organisms and, more
449 generally, how they may support pools of proliferating stem or progenitor cells in other
450 organisms and organ contexts. Moreover, since vitellogenin-like molecules, such as
451 ApoB, are implicated in heart disease and other aspects of lipid metabolism (reviewed in
452 (Sniderman et al., 2019)), the *C. elegans* larval germ line may provide inroads to the
453 identification of additional associated moieties and receptors.
454

455 **ACKNOWLEDGMENTS**
456 We thank the Microscopy (RRID: SCR_017934) and Genome Technology (RRID:
457 SCR_017929) cores at NYU Grossman School of Medicine. The Microscopy Core is
458 partially supported by the Cancer Center Support Grant P30CA016087 and
459 P01A1080192 at the Laura and Isaac Perlmutter Cancer Center. The Genome
460 Technology Core is partially supported by the Cancer Center Support Grant
461 P30CA016087 at the Laura and Isaac Perlmutter Cancer Center. We thank Nicole Hall
462 for help and advice with the RNA extraction protocol and analysis, Amy Webster for
463 feedback on the RNA-seq analysis, Sophie Wasel and Mia Sinks for technical support,
464 and Michael Cammer for microscopy support. We are also grateful for feedback and
465 support from Jeremy Nance and Niels Ringstad, and members of their labs. The
466 computational requirements for this work were supported in part by the NYU Langone
467 High Performance Computing (HPC) Core's resources and personnel. Thanks to Michael
468 O'Donnell for providing strains; some strains were also provided by the CGC, which is
469 funded by NIH Office of Research Infrastructure Programs (P40 OD010440). This work
470 was supported by NYSTEM Institutional Training Grant Contract #C322560GG and NIH
471 R35GM134876 to E.J.A.H., and a postdoctoral fellowship by the American Heart
472 Association to AK (https://doi.org/10.58275/AHA.25POST1362264.pc.gr.227408).
473
474 Competing Interests: The authors declare no competing interests.

475 **MATERIALS AND METHODS**

476 **Worm maintenance and husbandry**

477 *C. elegans* nematodes were grown on NGM solid media at 20°C and fed *Escherichia coli*
478 strain OP50 (Stiernagle, 2006). All strains generated and used in this study are listed with
479 full genotypes in Table S1, including the oligonucleotides used for strain validation. The
480 sequences of these oligonucleotides are listed in Table S2. Some strains were provided
481 by the CGC. All strains were based on Bristol N2 (RRID:WBSTRAIN:
482 WBStrain00000001). Many experiments required access to information on WormBase
483 (Sternberg et al., 2024). The following strains were generated in this study: GC1745,
484 GC1746, GC1747, GC1755, GC1756, GC1759, GC1762, GC1764, GC1779, GC1779,

485 GC1780, GC1793, GC1801, GC1802, GC1815, GC1816, GC1829, GC1832, GC1842,
486 GC1886, GC1893, GC1905.
487

488 **Determination of progenitor zone nuclei counts and mitotic index**

489 Mid-L4 worms (L4.5; (Mok et al., 2015)) were picked from mixed stage plates and
490 transferred to new plates. 6h later all early adult worms bearing a vulval slit were picked
491 into 1ml of M9+Tween within a 1.5ml of low-retention microfuge tube (02-681-320,
492 Fisherbrand). Worms were spun down on a table-top centrifuge for 10 seconds, before
493 the supernatant was carefully removed with a pipette under the dissecting scope, to avoid
494 loss of worms. Another 500µl of M9+Tween was added, followed by a centrifugation and
495 supernatant removal. 50µl of 100%EtOH were added to each sample, and worms were
496 allowed to settle at the bottom for ~10min. After 10min as much EtOH was removed as
497 possible without disturbing the worms, and ~5µl of Vectashield+DAPI (H-1000, Vector
498 Laboratories) was added. Worms were gently pipetted onto a 4% agar pad on a glass
499 slide. Slides were kept in the cold and dark and were imaged within 2 weeks after staining.
500 Imaging was performed on Nikon W1 spinning disk confocal microscope with 60x oil
501 immersion magnification with z-stacks of 0.5µm step size. Only one gonad arm was
502 counted per individual worm. PZ nuclei were manually counted using the point tool in
503 ImageJ (Arganda-Carreras et al., 2024). The PZ border was determined as the distal-
504 most row with 2 or more crescent-shaped nuclei typical of the transition zone (Crittenden
505 et al., 2006). Mitotic index is presented as a percentage of the number of mitotic figures
506 (characteristic metaphase and anaphase figures) divided by the total number of PZ nuclei.
507

508 **Brood Size Determination**

509 L4 worms were picked from mixed stage plates. Single hermaphrodites were added to
510 plates and, for the mated treatment, were joined by 3 wild-type males, which were
511 replaced every two days. In mating experiments (Fig. S1), mating was confirmed by
512 abundant male offspring (N2 males) and/or mating plug (CB4855 males). Mated
513 *rict-1(-)* hermaphrodites exhibited poorer survival than self-fertile hermaphrodites;
514 however, offspring counts are included only from worms that lived several days after the

515 last progeny were produced (see Fig. S1). All worms were transferred every day to new
516 plates, and hatched offspring were counted 2 days later.

517 **CRISPR-Cas9 genome editing**

518 CRISPR/Cas9 genome editing was performed using pre-incubated Cas9
519 (Berkeley)::(crRNA +tracrRNA) (IDT) ribonucleoprotein, and screening was facilitated by
520 co-CRISPR detection using the *dpy-10(cn64)* mutation as described (Paix et al., 2017).
521 DNA repair templates contained ~25–35 bps of homology on each arm as ssDNA oligos
522 (<150 bps) (IDT). The guide RNAs and oligos are listed in Table S3. For Stop-In mutants
523 (*na112, na113, na114*, and *na115*) the inserted stop cassette led to an early stop in all
524 frames (Wang et al., 2018), while the sAID tag did not interfere with the function of RICT-
525 1 (Fig. S3B).

526 **Integration of extrachromosomal array**

527 The extrachromosomal array *oyEx713* in GC1756 was integrated using x-rays, as
528 previously described (Evans, 2006).
529

530 **RNA extraction for bulk RNA-seq**

531 Worms were bleached and synchronized as previously described (Stiernagle, 2006). Due
532 to differences in growth rate (as previously empirically determined), synchronized L1
533 larvae were added to 15 10cm NGM plates (each inoculated with 1ml of OP50) at different
534 times so that all strains would reach the mid-L4 stage at the same time. Worms were
535 washed off the plates with RNAse-free water (10977015, Invitrogen) and collected atop
536 pluristrainers with 40µl mesh size (#43-10040-40 from Pluristrainer.com) and washed
537 three times with 5ml of RNAse free H_20. Pluristrainers were turned over, and 1ml of
538 RNAse-free water was used to wash the worms off the mesh and collect them in RNAse-
539 free 2ml Eppendorf microfuge tubes (E0030123620, Eppendorf). Each 1ml of packed
540 worms was resuspended in 4ml of Trizol. The worm+Trizol mix was vortexed and flash-
541 frozen by carefully dropping into liquid nitrogen and then thawed at 37ºC. After three
542 freeze-thaw cycles, samples were thawed at 37ºC, and 2ml of Trizol+2ml of chloroform

543 per packed ml of worms was added and vigorously shaken by hand. Samples were
544 aliquoted into 2ml RNAse-free tubes and incubated at room temperature for three
545 minutes. Samples were then spun at 12,000g at 4ºC for 15 min. The aqueous layer was
546 removed into new RNAse-free tubes, and an equal volume of 70% ethanol was added
547 and inverted to mix. This solution was transferred to a spin column (RNeasy Qiagen kit #
548 74104) and was spun down at 21k rcf for 30sec. The column was washed once with buffer
549 RW1 and centrifuged for 15 seconds at 21k rcf DNase I was added directly to each
550 RNeasy column membrane and was left to incubate at room temperature for 15 minutes.
551 Each column was washed with Qiagen RW1 and RPE buffers, before the sample was
552 eluted from the spin column in RNase-free water to be collected in a fresh 2ml RNase-
553 free tube. RNA quality was initially assessed with a nanodrop (NanoDrop 8000 UV-Vis
554 Spectrophotometer). Samples were submitted to the NYU genome technology core
555 where RNA extractions were quantified using RNA Nano Chips (Cat. #5067-1511) on an
556 Agilent 2100 BioAnalyzer. RNA-Seq library preps were constructed with the Illumina
557 TruSeq Stranded mRNA Library Prep kit (Cat #20020595) according to manufacturer's
558 recommendations. The input amount of total RNA was 450ng with 12 cycles of
559 amplification. Final libraries were visualized using High Sensitivity DNA ScreenTape
560 (Agilent, Cat. #5067-5584) on the Agilent TapeStation 2200 instrument. Quant-It
561 (Invitrogen, Cat. P11495) was used for concentration determination and libraries were
562 pooled equimolar. The pool was sequenced paired-end 50 cycles on an Illumina NovaSeq
563 X+ 10B 100 cycle flowcell with 2% PhiX spike-in.
564
565 **RNA-seq analysis**
566 Version WBCel235 of the *C. elegans* genome was used to map sequencing reads (Table
567 S4). Seq-N-Slide (Dolgalev, 2024) was used to align the sequencing results and
568 determine those gene transcripts that are differentially expressed between the mutant
569 and wild-type strains. Transcript counts were restricted to protein coding genes (19,983
570 genes). Mapping Efficiency is provided in Table S5. Prior to further analysis this count
571 data was further restricted to include only genes represented in at least 2/3 libraries per
572 strain with non-zero counts (16,034 genes). Principal component analysis (PCA) was
573 performed on log2 normalized CPM values on all genes included in the differential gene

expression analysis (16,034 genes), using the stats package in R (version 2024.04.2+764) (RStudio Team, 2020). Lists of genes with differentially abundant transcripts between WT versus *rict-1* and *rict-1* versus *rict-1; Is[intestinal rict-1(+)]* can be found in Table S4. The entire dataset will be publicly available at NCBI Gene Expression Omnibus.

Statistical analyses

Plots in Figures 1-6 and Figures S1-S3 were generated using R with minor modifications using Adobe Illustrator or Inkscape. Statistical analysis was conducted in R (version 2024.04.2+764) (RStudio Team, 2020). All PZ counts and the offspring data were analyzed with a Generalized Mixed Effect Model (Nelder and Wedderburn, 1972), taking the replicate as a random factor into account. The Mitotic Index data was analyzed using a Linear Model (Nelder and Wedderburn, 1972), and the Reproductive Period data was analyzed with a Linear Mixed Effects Model (Nelder and Wedderburn, 1972). All results from the statistical tests can be found in Table S6 and all detailed p-values can be found in Table S7. Summaries of all data are in Table S8.

Conceptualization: A.K., E.J.A.H.;
Formal analysis: A.K.
Funding acquisition: A.K., E.J.A.H.;
Investigation: A.K.
Methodology: A.K., E.J.A.H.;
Project administration: E.J.A.H.;
Supervision: E.J.A.H.;
Visualization: A.K.
Writing original draft: A.K.
Writing – review & editing: A.K., E.J.A.H.;

604 **Abete-Luzi, P., Fukushige, T., Yun, S., Krause, M. W. and Eisenmann, D. M.** (2020). New
605 Roles for the Heterochronic Transcription Factor LIN-29 in Cuticle Maintenance and
606 Lipid Metabolism at the Larval-to-Adult Transition in *Caenorhabditis elegans*. *Genetics*
607 **214**, 669–690.

608 **Agarwal, I., Farnow, C., Jiang, J., Kim, K.-S., Leet, D. E., Solomon, R. Z., Hale, V. A. and**
609 **Goutte, C.** (2018). HOP-1 Presenilin Deficiency Causes a Late-Onset Notch Signalling
610 Phenotype That Affects Adult Germline Function in *Caenorhabditis elegans*. *Genetics*
611 **208**, 745–762.

612 **Arganda-Carreras, I., Barnhill, E., Doube, M., Eglinger, J., Entrup, M., Ferreira, T.,**
613 **Hiner, M., Landini, G. and Lloyd, C.** (2024). ImageJ and Fiji.

614 **Aspernig, H., Heimbucher, T., Qi, W., Gangurde, D., Curic, S., Yan, Y., Donner von**
615 **Gromoff, E., Baumeister, R. and Thien, A.** (2019). Mitochondrial Perturbations Couple
616 mTORC2 to Autophagy in *C. elegans*. *Cell Reports* **29**, 1399-1409.e5.

617 **Aupérin, N., Singh, M., Bourdon, L., Chervova, A., Commere, P.-H., Lopez-Maestre, H.,**
618 **Dingli, F., Loew, D., Ovieve, J. and Cecere, G.** (2025). Soma-to-Germline miRNA
619 inheritance via Yolk Promotes Stress Resilience in Progeny.

620 **Bhoi, A., Palladino, F. and Fabrizio, P.** (2021). Auxin confers protection against ER stress in
621 *Caenorhabditis elegans*. *Biology Open* **10**, bio057992.

622 **Blackwell, T. K., Sewell, A. K., Wu, Z. and Han, M.** (2019). TOR Signaling in *Caenorhabditis*
623 *elegans* Development, Metabolism, and Aging. *Genetics* **213**, 329–360.

624 **Boeck, M. E., Huynh, C., Gevirtzman, L., Thompson, O. A., Wang, G., Kasper, D. M.,**
625 **Reinke, V., Hillier, L. W. and Waterston, R. H.** (2016). The time-resolved
626 transcriptome of *C. elegans*. *Genome Res.* **26**, 1441–1450.

627 **Breen, P. C., Kanakanui, K. G., Newman, M. A. and Dowen, R. H.** (2024). The F-box protein
628 FBXL-5 governs vitellogenesis and lipid homeostasis in C. elegans. *Front. Cell Dev.*
629 *Biol.* **12**, 1389077.

630 **Cao, J., Packer, J. S., Ramani, V., Cusanovich, D. A., Huynh, C., Daza, R., Qiu, X., Lee, C.,**
631 **Furlan, S. N., Steemers, F. J., et al.** (2017). Comprehensive single-cell transcriptional
632 profiling of a multicellular organism. *Science* **357**, 661–667.

633 **Caron, A., Richard, D. and Laplante, M.** (2015). The Roles of mTOR Complexes in Lipid
634 Metabolism. *Annu. Rev. Nutr.* **35**, 321–348.

635 **Chen, J., Mohammad, A., Pazdernik, N., Huang, H., Bowman, B., Tycksen, E. and Schedl,**
636 **T.** (2020). GLP-1 Notch—LAG-1 CSL control of the germline stem cell fate is mediated
637 by transcriptional targets lst-1 and sygl-1. *PLoS Genet* **16**, e1008650.

638 **Crittenden, S. L., Leonhard, K. A., Byrd, D. T. and Kimble, J.** (2006). Cellular Analyses of
639 the Mitotic Region in the *Caenorhabditis elegans* Adult Germ Line. *MBoC* **17**, 3051–
640 3061.

641 **Dalfó, D., Michaelson, D. and Hubbard, E. J. A.** (2012). Sensory Regulation of the *C. elegans*
642 Germline through TGF-β-Dependent Signaling in the Niche. *Current Biology* **22**, 712–
643 719.

644 **Dolgalev, I.** (2024). Seq-N-Slide.

645 **Dowen, R. H., Breen, P. C., Tullius, T., Conery, A. L. and Ruvkun, G.** (2016). A microRNA
646 program in the *C. elegans* hypodermis couples to intestinal mTORC2/PQM-1 signaling to
647 modulate fat transport. *Genes Dev.* **30**, 1515–1528.

648 **Emans, S. W., Yerevanian, A., Ahsan, F. M., Rotti, J., Zhou, Y., Cedillo, L. and Soukas, A.**
649 **A.** (2023). *C. elegans* hedgehog/patched-like morphogen-receptor pair GRD-1/PTR-11
650 modulates developmental rate. *Development* dev.201974.

651 **Evans, T.** (2006). Transformation and microinjection. *WormBook*.

652 **Fox, P. M. and Schedl, T.** (2015). Analysis of Germline Stem Cell Differentiation Following
653 Loss of GLP-1 Notch Activity in *Caenorhabditis elegans*. *Genetics* **201**, 167–184.

654 **Frei, I. C., Weissenberger, D., Müller, C., Hall, M. N. and Shimobayashi, M.** (2023). Hepatic
655 mTORC2 compensates for loss of adipose mTORC2 in mediating energy storage and
656 glucose homeostasis. *American Journal of Physiology-Endocrinology and Metabolism*
657 **324**, E589–E598.

658 **Gatsi, R., Schulze, B., Rodríguez-Palero, M. J., Hernando-Rodríguez, B., Baumeister, R.**
659 **and Artal-Sanz, M.** (2014). Prohibitin-Mediated Lifespan and Mitochondrial Stress
660 Implicate SGK-1, Insulin/IGF and mTORC2 in *C. elegans*. *PLoS ONE* **9**, e107671.

661 **Ghaddar, A., Armingol, E., Huynh, C., Gevirtzman, L., Lewis, N. E., Waterston, R. and**
662 **O'Rourke, E. J.** (2023). Whole-body gene expression atlas of an adult metazoan.
663 *Science Advances* **9**,.

664 **Grant, B. and Hirsh, D.** (1999). Receptor-mediated Endocytosis in the *Caenorhabditis elegans*
665 Oocyte. *MBoC* **10**, 4311–4326.

666 **Guertin, D. A., Guntur, K. V. P., Bell, G. W., Thoreen, C. C. and Sabatini, D. M.** (2006).
667 Functional genomics identifies TOR-regulated genes that control growth and division.
668 *Current Biology* **16**, 958–970.

669 **Guri, Y., Colombi, M., Dazert, E., Hindupur, S. K., Roszik, J., Moes, S., Jenoe, P., Heim,**
670 **M. H., Riezman, I., Riezman, H., et al.** (2017). mTORC2 Promotes Tumorigenesis via
671 Lipid Synthesis. *Cancer Cell* **32**, 807-823.e12.

672 **Heine, U. and Blumenthal, T.** (1986). Characterization of regions of the *Caenorhabditis*
673 *elegans* X chromosome containing vitellogenin genes. *Journal of Molecular Biology* **188**,
674 301–312.

675 **Hietakangas, V. and Cohen, S. M.** (2007). Re-evaluating AKT regulation: role of TOR
676 complex 2 in tissue growth. *Genes & Development* **21**, 632–637.

677 **Hillier, L. W., Reinke, V., Green, P., Hirst, M., Marra, M. A. and Waterston, R. H.** (2009).
678 Massively parallel sequencing of the polyadenylated transcriptome of *C. elegans*.
679 *Genome Res.* **19**, 657–666.

680 **Hodgkin, J. and Barnes, T.** (1991). More is not better: brood size and population growth in a
681 self-fertilizing nematode. *Proc. R. Soc. Lond. B* **246**, 19–24.

682 **Hubbard, E. J. and Schedl, T.** (2019). Biology of the *Caenorhabditis elegans* Germline Stem
683 Cell System. *Genetics* **213**, 1145–1188.

684 **Hutter, H. and Suh, J.** (2016). GExplore 1.4: An expanded web interface for queries on
685 *Caenorhabditis elegans* protein and gene function. *Worm* **5**, e1234659.

686 **Jang, H., Park, Y. and Jang, J.** (2022). Serum and glucocorticoid-regulated kinase 1: Structure,
687 biological functions, and its inhibitors. *Front. Pharmacol.* **13**, 1036844.

688 **Jones, K. T., Greer, E. R., Pearce, D. and Ashrafi, K.** (2009). Rictor/TORC2 Regulates
689 *Caenorhabditis elegans* Fat Storage, Body Size, and Development through *sgk-1*. *PLoS*
690 *Biol* **7**, e1000060.

691 **Kershner, A. M., Shin, H., Hansen, T. J. and Kimble, J.** (2014). Discovery of two GLP-
692 1/Notch target genes that account for the role of GLP-1/Notch signaling in stem cell
693 maintenance. *Proc Natl Acad Sci USA* **111**, 3739–3744.

694 **Killian, D. J. and Hubbard, E. J. A.** (2004). *C. elegans pro-1* activity is required for
695 soma/germline interactions that influence proliferation and differentiation in the germ
696 line. *Development* **131**, 1267–1278.

697 **Kim, J. E. and Chen, J.** (2004). Regulation of Peroxisome Proliferator–Activated Receptor-
698 Delta Activity by Mammalian Target of Rapamycin and Amino Acids in Adipogenesis.
699 *Diabets* **53**,.

700 **Kimble, J. and Sharrock, W. J.** (1983). Tissue-specific synthesis of yolk proteins in
701 *Caenorhabditis elegans*. *Developmental Biology* **96**, 189–196.

702 **Kocsisova, Z., Kornfeld, K. and Schedl, T.** (2019). Rapid population-wide declines in stem cell
703 number and activity during reproductive aging in *C. elegans*. *Development* **146**, 15.

704 **Korta, D. Z., Tuck, S. and Hubbard, E. J. A.** (2012). S6K links cell fate, cell cycle and
705 nutrient response in *C. elegans* germline stem/progenitor cells. *Development* **141**, 236–
706 236.

Liu, G. Y. and Sabatini, D. M. (2020). mTOR at the nexus of nutrition, growth, ageing and disease. *Nat Rev Mol Cell Biol* **21**, 183–203.

Loose, J. A. and Ghazi, A. (2021). Auxin treatment increases lifespan in *Caenorhabditis elegans*. *Biology Open* **10**, bio058703.

McLachlan, I. G., Kramer, T. S., Dua, M., DiLoreto, E. M., Gomes, M. A., Dag, U., Srinivasan, J. and Flavell, S. W. (2022). Diverse states and stimuli tune olfactory receptor expression levels to modulate food-seeking behavior. *eLife* **11**, e79557.

Michaelson, D., Korta, D. Z., Capua, Y. and Hubbard, E. J. A. (2010). Insulin signaling promotes germline proliferation in *C. elegans*. *Development* **141**, 237–237.

Mohammad, A., Vanden Broek, K., Wang, C., Daryabeigi, A., Jantsch, V., Hansen, D. and Schedl, T. (2018). Initiation of Meiotic Development Is Controlled by Three Post-transcriptional Pathways in *Caenorhabditis elegans*. *Genetics* **209**, 1197–1224.

Mok, D. Z. L., Sternberg, P. W. and Inoue, T. (2015). Morphologically defined sub-stages of *C. elegans* vulval development in the fourth larval stage. *BMC Dev Biol* **15**, 26.

Nelder, J. A. and Wedderburn, R. W. M. (1972). Generalized Linear Models. *Journal of the Royal Statistical Society. Series A (General)* **135**, 370.

O'Donnell, M. P., Chao, P.-H., Kammenga, J. E. and Sengupta, P. (2018). Rictor/TORC2 mediates gut-to-brain signaling in the regulation of phenotypic plasticity in *C. elegans*. *PLoS Genet* **14**, e1007213.

Paix, A., Folkmann, A. and Seydoux, G. (2017). Precision genome editing using CRISPR-Cas9 and linear repair templates in *C. elegans*. *Methods* **121–122**, 86–93.

Pekar, O., Ow, M. C., Hui, K. Y., Noyes, M. B., Hall, S. E. and Hubbard, E. J. A. (2017). Linking the environment, DAF-7/TGFβ signaling and LAG-2/DSL ligand expression in the germline stem cell niche. *Development* **144**, 2896–2906.

Perez, M. F. and Lehner, B. (2019). Vitellogenins - Yolk Gene Function and Regulation in *Caenorhabditis elegans*. *Front. Physiol.* **10**, 1067.

Puca, F., Fedele, M., Rasio, D. and Battista, S. (2022). Role of Diet in Stem and Cancer Stem Cells. *IJMS* **23**, 8108.

Roy, D., Michaelson, D., Hochman, T., Santella, A., Bao, Z., Goldberg, J. D. and Hubbard, E. J. A. (2016). Cell cycle features of *C. elegans* germline stem/progenitor cells vary temporally and spatially. *Developmental Biology* **409**, 261–271.

Roy, D., Kahler, D. J., Yun, C. and Hubbard, E. J. A. (2018). Functional Interactions Between *rsks-1* /S6K, *glp-1* /Notch, and Regulators of *Caenorhabditis elegans* Fertility and Germline Stem Cell Maintenance. *G3 Genes|Genomes|Genetics* **8**, 3293–3309.

741 **RStudio Team** (2020). RStudio.

742 **Ruf, V., Holzem, C., Peyman, T., Walz, G., Blackwell, T. K. and Neumann-Haefelin, E.**
743 (2013). TORC2 signaling antagonizes SKN-1 to induce *C. elegans* mesendodermal
744 embryonic development. *Developmental Biology* **384**, 214–227.

745 **Russell, R. C., Fang, C. and Guan, K.-L.** (2011). An emerging role for TOR signaling in
746 mammalian tissue and stem cell physiology. *Development* **138**, 3343–3356.

747 **Saba, J. A., Liakath-Ali, K., Green, R. and Watt, F. M.** (2021). Translational control of stem
748 cell function. *Nat Rev Mol Cell Biol* **22**, 671–690.

749 **Sakai, N., Ohno, H., Tomioka, M. and Iino, Y.** (2017). The intestinal TORC2 signaling
750 pathway contributes to associative learning in *Caenorhabditis elegans*. *PLoS ONE* **12**,
751 e0177900.

752 **Salinas, L. S., Maldonado, E., Macías-Silva, M., Blackwell, T. K. and Navarro, R. E.** (2007).
753 The DEAD box RNA helicase VBH-1 is required for germ cell function in *C. elegans*.
754 *Genesis* **45**, 533–546.

755 **Shin, H., Haupt, K. A., Kershner, A. M., Kroll-Conner, P., Wickens, M. and Kimble, J.**
756 (2017). SYGL-1 and LST-1 link niche signaling to PUF RNA repression for stem cell
757 maintenance in *Caenorhabditis elegans*. *PLoS Genet* **13**, e1007121.

758 **Sniderman, A. D., Thanassoulis, G., Glavinovic, T., Navar, A. M., Pencina, M., Catapano,**
759 **A. and Ference, B. A.** (2019). Apolipoprotein B Particles and Cardiovascular Disease: A
760 Narrative Review. *JAMA Cardiol* **4**, 1287.

761 **Soukas, A. A., Kane, E. A., Carr, C. E., Melo, J. A. and Ruvkun, G.** (2009). Rictor/TORC2
762 regulates fat metabolism, feeding, growth, and life span in *Caenorhabditis elegans*.
763 *Genes Dev.* **23**, 496–511.

764 **Sternberg, P. W., Van Auken, K., Wang, Q., Wright, A., Yook, K., Zarowiecki, M.,**
765 **Arnaboldi, V., Becerra, A., Brown, S., Cain, S., et al.** (2024). WormBase 2024: status
766 and transitioning to Alliance infrastructure. *GENETICS* **227**, iyae050.

767 **Stiernagle, T.** (2006). Maintenance of *C. elegans*. *WormBook*.

768 **Szwed, A., Kim, E. and Jacinto, E.** (2021). Regulation and metabolic functions of mTORC1
769 and mTORC2. *Physiological Reviews* **101**, 1371–1426.

770 **Tu, W. B., Christofk, H. R. and Plath, K.** (2023). Nutrient regulation of development and cell
771 fate decisions. *Development* **150**, dev199961.

772 **VanDerMolen, K. R., Newman, M. A., Breen, P. C., Huff, L. A. and Dowen, R. H.** (2025).
773 Non-cell-autonomous regulation of mTORC2 by Hedgehog signaling maintains lipid
774 homeostasis. *Cell Reports*.

775 **Wang, H., Park, H., Liu, J. and Sternberg, P. W.** (2018). An Efficient Genome Editing
776 Strategy To Generate Putative Null Mutants in *Caenorhabditis elegans* Using
777 CRISPR/Cas9. *G3 Genes|Genomes|Genetics* **8**, 3607–3616.

778 **Webster, C. M., Wu, L., Douglas, D. and Soukas, A. A.** (2013). A non-canonical role for the
779 *C. elegans* dosage compensation complex in growth and metabolic regulation
780 downstream of TOR complex 2. *Development* **140**, 3601–3612.

781 **Yen, K., Le, T. T., Bansal, A., Narasimhan, S. D., Cheng, J.-X. and Tissenbaum, H. A.**
782 (2010). A Comparative Study of Fat Storage Quantitation in Nematode *Caenorhabditis*
783 *elegans* Using Label and Label-Free Methods. *PLoS ONE* **5**, e12810.

784 **Zhang, L., Ward, J. D., Cheng, Z. and Dernburg, A. F.** (2015). The auxin-inducible
785 degradation (AID) system enables versatile conditional protein depletion in *C. elegans*.
786 *Development* dev.129635.

787 **Zoncu, R., Efeyan, A. and Sabatini, D. M.** (2011). mTOR: from growth signal integration to
788 cancer, diabetes and ageing. *Nat Rev Mol Cell Biol* **12**, 21–35.

789

FIGURES + FIGURE LEGENDS

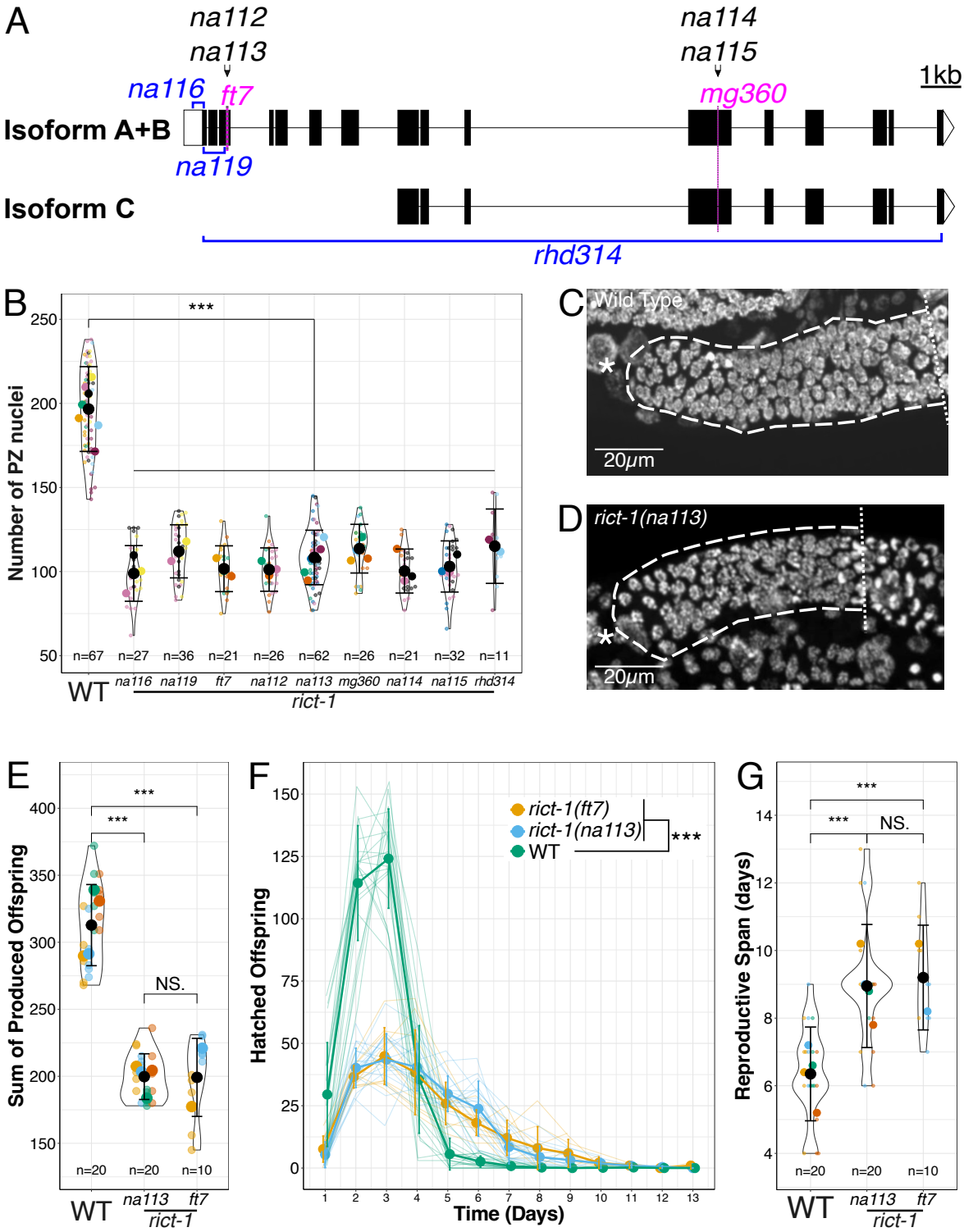

Figure 1: *rict-1* regulates reproduction and the germline progenitor zone. (A) Overview of the nine different *rict-1* mutants used in this study (two SNP mutations in magenta, four Stop-in mutants in black, and three knock-out mutants in blue). Scale bar indicates 1kb.

795 Alleles *mg360*, *na114*, *na115,* and *rhd314* affect all isoforms. (B) Number of PZ nuclei for
796 wild type and nine tested *rict-1* mutants. (C, D) Micrographs of representative wild type
797 (C) and *rict-1(na113)* mutant (D) progenitor zones. (E) Average of hatched offspring per
798 adult over a lifetime. (F) Hatched offspring per adult over time; the thick lines indicate the
799 average per strain, while the thinner lines indicate single worms. Error bars indicate
800 standard error of the mean. (G) Reproductive period in days. (B, E, G) Black circles
801 indicate the means across independent replicate experiments (these replicate
802 experiments are shown in different colors), while the smallest circles indicate gonad arms
803 (n = number of gonad arms scored), also summarized below each violin. The violin
804 displays the overall distribution of data points. Error bars indicate the standard error of
805 the mean. Statistical results and p-values are summarized in Tables S6 and S7,
806 respectively. The asterisks indicate *** $p<0.001$, ** $p<0.01$, * $p<0.05$. Panel B, E, and G
807 were analyzed with a Linear Mixed Effects Model, Panel F was analyzed with a
808 Generalized Linear Model, followed up with a Tukey Post Hoc test where appropriate.
809

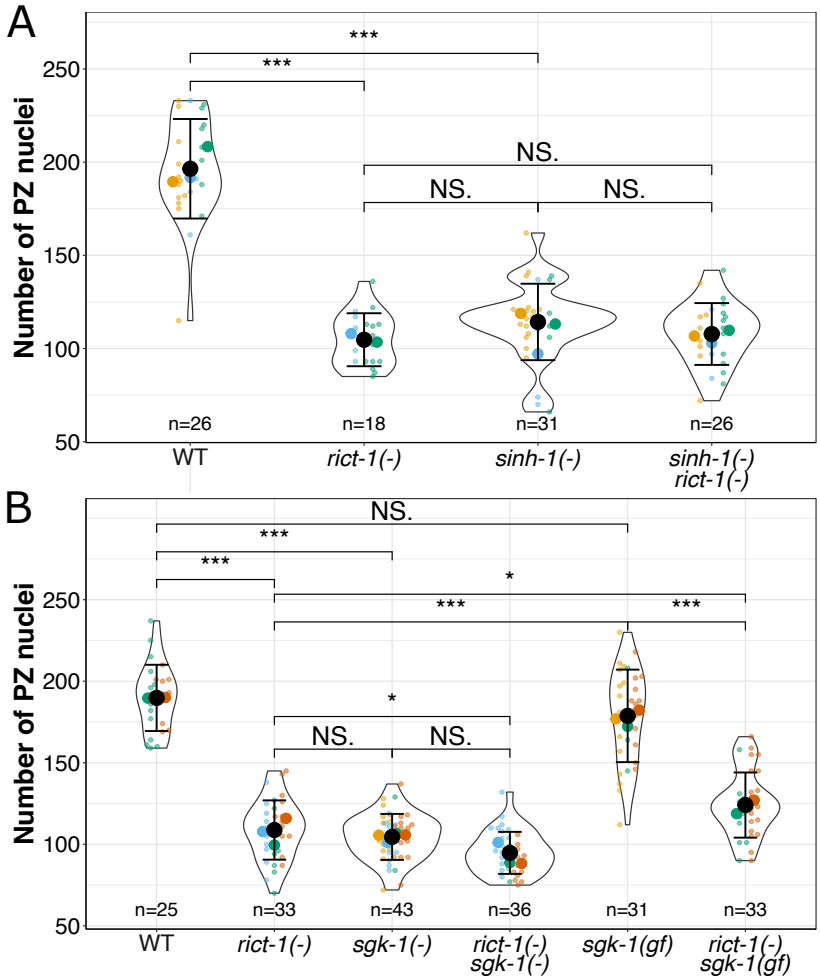

Figure 2: RICT-1 likely acts via canonical TORC2 signaling pathway. (A, B) Number of PZ nuclei in the wild type (WT) and indicated mutant genotypes. Black circles indicate the means across independent replicate experiments (these replicate experiments are shown in different colors), while the smallest circles indicate gonad arms (n = number of gonad arms scored), also summarized below each violin. The violin displays the overall distribution of data points. Error bars indicate the standard error of the mean. Statistical results and p-values are summarized in Tables S6 and S7, respectively. The asterisks indicate *** $p<0.001$, ** $p<0.01$, * $p<0.05$. The asterisks indicate *** $p<0.001$, ** $p<0.01$, * $p<0.05$ of a Linear Mixed Effects Model with a Tukey Post Hoc Test.

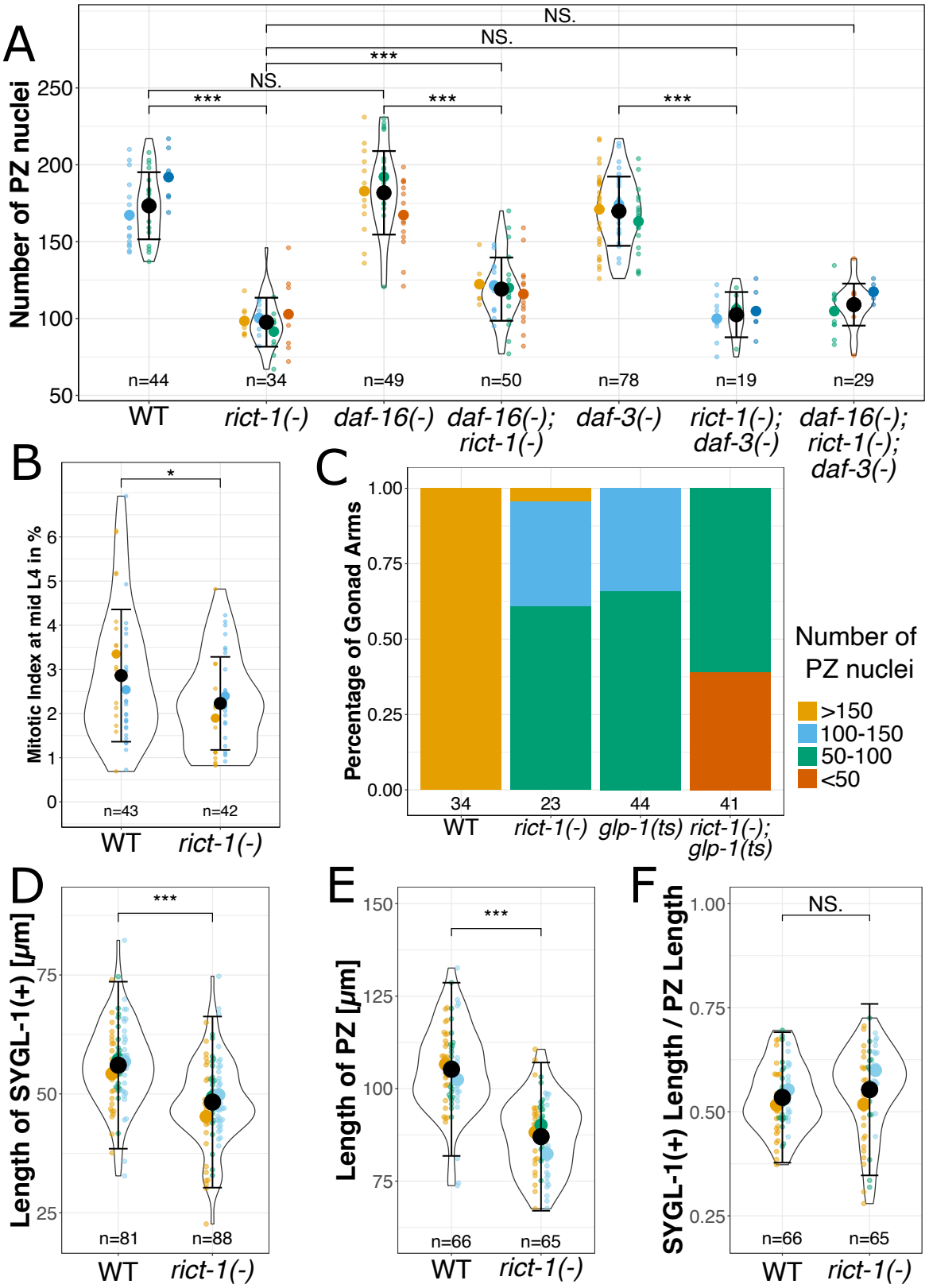

Figure 3: RICT-1 does not act via the IIS or the DAF-7/TGF-ß pathway but regulates larval cell cycle and not stem cell fate. (A) Number of PZ nuclei in the wild type (WT) and

825 indicated mutants. (B) Mitotic index at the mid-L4 in the WT and *rict-1(-)* mutant. (C) The
826 percentage of gonad arms displaying the indicated range in numbers of PZ nuclei. (D, E,
827 F) The Length of the SYGL-1(+) (D) and PZ (E) zones, and their ratio (F) in WT and *rict-*
828 *1(-)* mutants. (A, B, D-F) Black circles indicate the means across independent replicate
829 experiments (these replicate experiments are shown in different colors), while the
830 smallest circles indicate gonad arms (n = number of gonad arms scored), also
831 summarized below each violin. The violin displays the overall distribution of data points.
832 Error bars indicate the standard error of the mean. Statistical results and
833 p-values are summarized in Tables S6 and S7, respectively. The asterisks indicate
834 *** $p<0.001$, ** $p<0.01$, * $p<0.05$ of a Linear Mixed Effects Model with a Tukey Post Hoc
835 Test. (C) Stacked bar plots represent the ratio of gonad arms that fall into different
836 categories, indicated on the right (yellow for gonad arms with >150 PZ nuclei, light blue
837 for gonad arms with 100-150 PZ nuclei, green for gonad arms with 50-100 PZ nuclei, and
838 orange for gonad arms with <50 PZ nuclei. Individual examined gonad arms are indicated
839 below each bar.
840

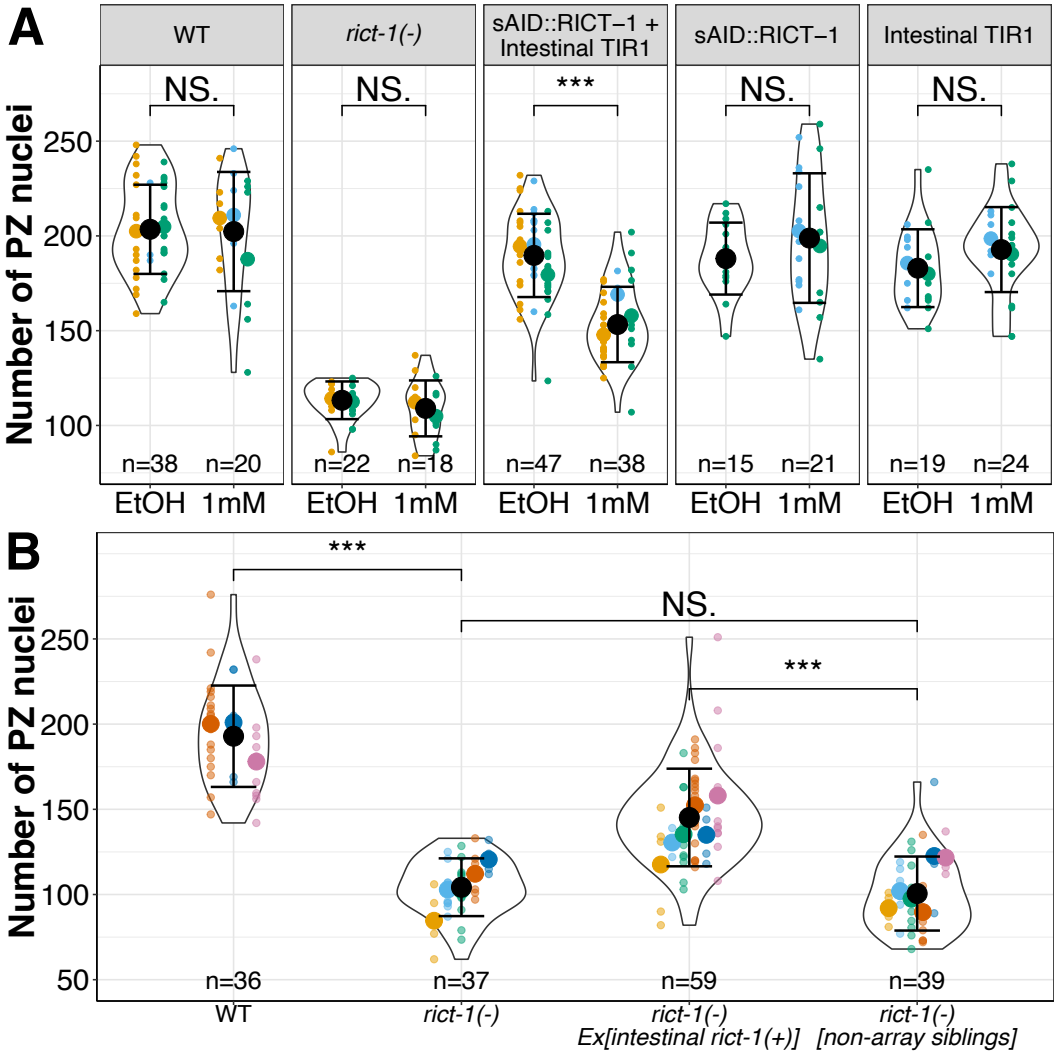

Figure 4: Intestinal RICT-1 is necessary and sufficient for full establishment of the PZ. (A) Numbers of PZ nuclei in the presence of the vehicle (EtOH) and auxin in the wild type (WT) and *rict-1(-)* and in strains bearing sAID::RICT-1 and/or the intestinal TIR1 (*ieSi61*). (B) Numbers of PZ nuclei in the wild type (WT) and in array bearing and non-array bearing sibling progeny from *rict-1(-)* mothers carrying (*oyEx713[ges-1p::rict-1(+)]*), an array that expresses *rict-1(+)* in the intestine. Black circles indicate the means across independent replicate experiments (these replicate experiments are shown in different colors), while the smallest circles indicate gonad arms (n = number of gonad arms scored), also summarized below each violin. The violin displays the overall distribution of data points. Error bars indicate the standard error of the mean. Statistical results and p-values are summarized in Tables S6 and S7, respectively. The asterisks indicate *** $p<0.001$, ** $p<0.01$, * $p<0.05$ of a Linear Mixed Effects Model with a Tukey Post Hoc Test.

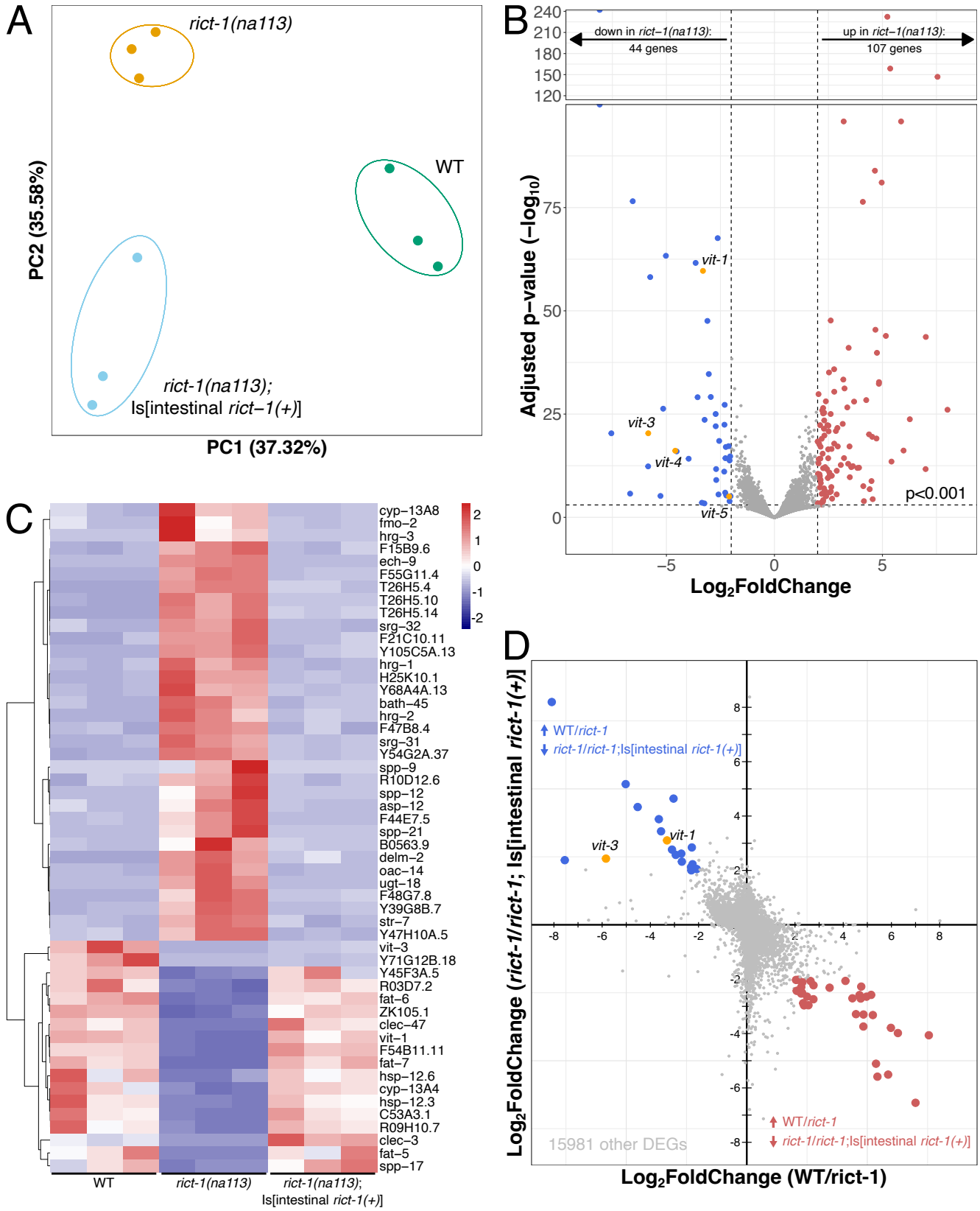
A
rict-1(na113)
WT
rict-1(na113);
Is[intestinal rict–1(+)]
PC2 (35.58%)
PC1 (37.32%)
B
down in rict–1(na113):
44 genes
up in rict–1(na113):
107 genes
Adjusted p–value (–log10)
vit-1
vit-3
vit-4
vit-5
p<0.001
Log2FoldChange
C
cyp–13A8
fmo–2
hrg–3
F15B9.6
ech–9
F55G11.4
T26H5.4
T26H5.10
T26H5.14
srg–32
F21C10.11
Y105C5A.13
hrg–1
H25K10.1
Y68A4A.13
bath–45
hrg–2
F47B8.4
srg–31
Y54G2A.37
spp–9
R10D12.6
spp–12
asp–12
F44E7.5
spp–21
B0563.9
delm–2
oac–14
ugt–18
F48G7.8
Y39G8B.7
str–7
Y47H10A.5
vit–3
Y71G12B.18
Y45F3A.5
R03D7.2
fat–6
ZK105.1
clec–47
vit–1
F54B11.11
fat–7
hsp–12.6
cyp–13A4
hsp–12.3
C53A3.1
R09H10.7
clec–3
fat–5
spp–17
WT
rict-1(na113)
rict-1(na113);
Is[intestinal rict-1(+)]
D
WT/rict-1
rict-1/rict-1;Is[intestinal rict-1(+)]
vit-3
vit-1
15981 other DEGs
Log2FoldChange (rict-1/rict-1; Is[intestinal rict-1(+)])
Log2FoldChange (WT/rict-1)

854

855 Figure 5: RNA-sequencing reveals that two vitellogenin encoding genes are regulated by
856 intestinal RICT-1. (A) Principal Component Analysis of the three strains, in which each
857 filled circle indicates one library, color coded by the three different strains. (B) Volcano
858 plot displaying a comparison of transcript abundance between *rict-1(-)* mutants and wild
859 type (WT) as circles in both the *rict-1(-)* mutant and the WT: not significantly regulated
860 (grey), down-regulated in the *rict-1(-)* mutant (blue – 107 genes) or up-regulated in the
861 *rict-1(-)* mutant (red – 44 genes) relative to WT. Vitellogenin genes are labeled and
862 marked in orange circles. The horizontal dashed line indicates the adjusted p-value
863 threshold of <0.001, while the vertical dashed lines indicate a log2 Fold Change of -2 or
864 2. (C) Heatmap in which each line indicates one differentially regulated gene (log2 fold
865 change >2 and adjusted p value < 0.001 – colored points from panel B) between WT, the
866 *rict-1(-),* and the *rict-1(-)* mutant with *Is[intestinal rict-1(+)].* The color scale indicates the
867 Fragments per Kilobase of transcript per Million mapped reads (FPKM), where darker
868 colors indicate a stronger differential, where blue colors indicate lower and red higher
869 abundance. (D) The fold change between WT and *rict-1(-)* is displayed on the x-axis and
870 fold change between *rict-1(-)* and *rict-1(-); Is[intestinal rict-1(+)]* are shown. Blue circles
871 indicate those transcripts of < -2 log2 Fold Change between WT and *rict-1(-)* and >2 Fold
872 Change between *rict-1(-)* and *rict-1(-); Is[intestinal rict-1(+))].* Red circles indicate those
873 transcripts of >2 log2 Fold Change between WT and *rict-1(-)* and < -2 Fold Change
874 between *rict-1(-)* and *rict-1(-); Is[intestinal rict-1(+))]. vit-1* and *vit-3* are labelled in orange
875 circles. Grey circles indicate those transcripts that did not fall into the above-mentioned
876 categories (15981 transcripts). All transcripts can be found in Table S4.
877

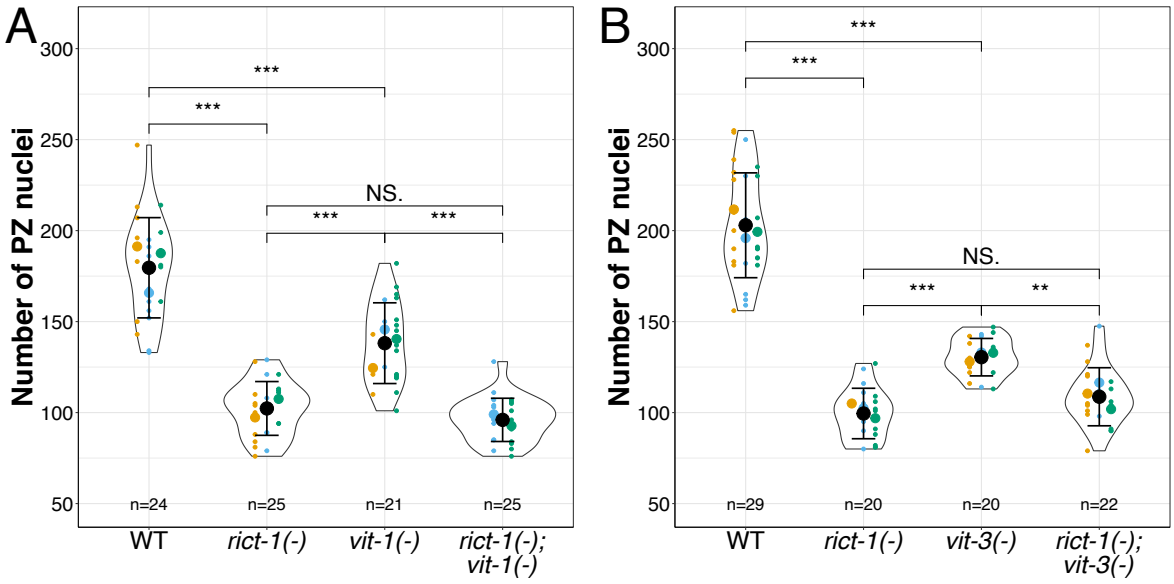

Figure 6: Two vitellogenins, VIT-1 and VIT-3, are likely acting in a linear pathway with RICT-1 to promote establishment of the PZ pool. (A, B) Numbers of PZ nuclei in the wild type (WT) and indicated genotypes. Black circles indicate the means across independent replicate experiments (these replicate experiments are shown in different colors), while the smallest circles indicate gonad arms (n = number of gonad arms scored), also summarized below each violin. The violin displays the overall distribution of data points. Error bars indicate the standard error of the mean. Statistical results and p-values are summarized in Tables S6 and S7, respectively. The asterisks indicate *** $p<0.001$, ** $p<0.01$, * $p<0.05$ of a Generalized Linear Model with a Tukey Post Hoc Test.